AMERICAN SOCIETY FOR MICROBIOLOGY | Antimicrobial Agents and Chemotherapy®

MECHANISMS OF RESISTANCE

Role of MurT C-Terminal Domain in the Amidation of *Staphylococcus aureus* Peptidoglycan

Bárbara V. Gonçalves,[a] Raquel Portela,[a] Ricardo Lobo,[a] Teresa A. Figueiredo,[a,b] Inês R. Grilo,[a] Ana Madalena Ludovice,[a] Hermínia de Lencastre,[b,d] Jorge S. Dias,[c] Rita G. Sobral[a]

[a]Laboratory of Molecular Microbiology of Bacterial Pathogens, UCIBIO@REQUIMTE, Departamento de Ciências da Vida, Faculdade de Ciências e Tecnologia, Universidade Nova de Lisboa, Caparica, Portugal

[b]Laboratory of Molecular Genetics, Instituto de Tecnologia Química e Biológica António Xavier, Universidade Nova de Lisboa, Oeiras, Portugal

[c](Bio)Molecular Structure and Interactions by NMR, UCIBIO@REQUIMTE, Departamento de Química, Faculdade de Ciências e Tecnologia, Universidade Nova de Lisboa, Caparica, Portugal

[d]Laboratory of Microbiology and Infectious Diseases, The Rockefeller University, New York, New York, USA

ABSTRACT Glutamate amidation, a secondary modification of the peptidoglycan, was first identified in *Staphylococcus aureus*. It is catalyzed by the protein products of the *murT* and *gatD* genes, which are conserved and colocalized in the genomes of most sequenced Gram-positive bacterial species. The MurT-GatD complex is required for cell viability, full resistance to β-lactam antibiotics, and resistance to human lysozyme and is recognized as an attractive target for new antimicrobials. Great effort has been invested in the study of this step, culminating recently in three independent reports addressing the structural elucidation of the MurT-GatD complex. In this work, we demonstrate through the use of nonstructural approaches the critical and multiple roles of the C-terminal domain of MurT, annotated as DUF1727, in the MurT-GatD enzymatic complex. This domain provides the physical link between the two enzymatic activities and is essential for the amidation reaction. Copurification of recombinant MurT and GatD proteins and bacterial two-hybrid assays support the observation that the MurT-GatD interaction occurs through this domain. Most importantly, we provide *in vivo* evidence of the effect of substitutions at specific residues in DUF1727 on cell wall peptidoglycan amidation and on the phenotypes of oxacillin resistance and bacterial growth.

KEYWORDS DUF1727, MurT-GatD, *Staphylococcus aureus*, antibiotic resistance, cell wall, peptidoglycan amidation

The biosynthesis of peptidoglycan, a major component of the cell wall of Gram-positive bacteria, begins in the cytoplasm with the synthesis of the sugar-linked pentapeptide, catalyzed by members of the Mur ligase family. At the membrane, this precursor is associated with bactoprenol to form lipid I and lipid II, which is translocated to the outer surface of the bacterium and incorporated into the cell wall (1). Most peptidoglycan synthesis-associated reactions are important targets for the most clinically relevant antibiotics, such as β-lactams and glycopeptides.

Chemical analysis of different bacterial species showed that the peptidoglycan undergoes several secondary modifications (2). In *Staphylococcus aureus*, these involve *O*-acetylation, attachment of teichoic acids (2), and amidation of the second residue of the pentapeptide (conversion of D-*iso*-glutamate into D-*iso*-glutamine). Although the role of these modifications is not fully understood, they are known to contribute to resistance against host defense, which impacts the virulence potential of the bacteria (3, 4).

The genes directly responsible for the amidation of glutamate, *murT* and *gatD*, were

Citation Gonçalves BV, Portela R, Lobo R, Figueiredo TA, Grilo IR, Ludovice AM, de Lencastre H, Dias JS, Sobral RG. 2019. Role of MurT C-terminal domain in the amidation of *Staphylococcus aureus* peptidoglycan. Antimicrob Agents Chemother 63:e00957-19. https://doi.org/10.1128/AAC.00957-19.

Address correspondence to Rita G. Sobral, rgs@fct.unl.pt.

B.V.G. and R.P. contributed equally to this article.

Received 9 May 2019
Returned for modification 2 June 2019
Accepted 20 July 2019
Accepted manuscript posted online 29 July 2019
Published 23 September 2019

identified in 2012 in *S. aureus* (5); they are widespread among Gram-positive bacteria, including important human pathogens. such as *Streptococcus pneumoniae*, *Enterococcus faecalis*, and *Mycobacterium* spp. (2, 6). We constructed the *S. aureus* conditional mutant COL*pCadmurT-gatD*, placing the chromosomal copy of the *murT-gatD* operon under the transcriptional control of the inducible promoter *pCad*. In the absence of inducer, the mutant strain showed altered phenotypes: a decreased growth rate, impaired β-lactam resistance, and increased susceptibility to the host defense factor lysozyme (5, 7).

The MurT and GatD proteins form a bienzymatic complex that catalyzes the amidation of lipid II (8). The MurT protein belongs to the Mur ligase family, and GatD is a glutamine amidotransferase (GATase)-like protein that shares the glutaminase motifs of GATase proteins, while it lacks the substrate binding domain and the ATP binding motif of these proteins (9–11).

Proteins of the Mur ligase family are typically composed of three domains: (i) an N-terminal domain, which is involved in binding of the UDP-MurNAc substrate; (ii) a central domain, which shows homology to the ATP binding domain of ATPases and GTPases; and (iii) a C-terminal domain, which is involved in the binding of the incoming amino acid (12, 13). The MurT protein shows 15% to 25% sequence identity and approximately 50% similarity to other members of the Mur ligase family. However, these values are mainly dependent on the central domain. The amino acid sequence of the C-terminal domain, annotated in the Pfam database as DUF1727 (InterPro accession number IPR013564), shows no extensive sequence similarity to any known protein domain and is always associated with the MurT protein.

In this communication, we describe the role of DUF1727 in MurT-GatD complex formation and *in vitro* activity. We explore the role of DUF1727 in *in vivo* complex activity by determining the levels of peptidoglycan amidation and their impact on the associated phenotypes, growth rates, and oxacillin resistance.

RESULTS

In this work, we describe the role of DUF1727 in the formation and activity of the MurT-GatD complex. The *murT-gatD* operon is essential for the survival of *S. aureus* under normal laboratory conditions, as has been described through an RNA interference approach (8). The molecular model system used in the present study consists of an *S. aureus* conditional mutant with the *murT-gatD* operon under the transcriptional control of the *pCad* inducible promoter (5). Use of the *pCad* promoter allows discrete levels of amidation to be studied. In the complete absence of the $CdCl_2$ inducer, we did not observe a complete arrest of growth, but we did observe a reduced growth rate as residual gene expression occurred. Genetic complementation of the conditional mutant was carried out by providing *murT* gene expression in *trans* by use of the replicative plasmid pSK*murT*. This resulted in partial phenotypic complementation of antibiotic resistance and the growth rate, even in the absence of GatD (5) (Fig. 1A and B).

DUF1727 is essential for MurT-GatD activity in *S. aureus*. The conditional mutant COL*pCadmurT-gatD* complemented with the *murT* gene encoded by pSK*murT* was used to address the role of DUF1727 in the amidation of the peptidoglycan of *S. aureus*. DUF1727 (Pfam accession number PF08353) is annotated in the Pfam database (http://pfam.xfam.org) as a domain of approximately 12 kDa delimited by residues L313 and S421 (see Fig. S1A in the supplemental material). The copy of the *murT* gene provided in *trans* was modified by site-directed mutagenesis (SDM) to replace the L313 residue with a stop codon, producing a truncated MurT protein which lacks the C-terminal domain (DUF1727). The resulting plasmid, pSK*murT*Δ*DUF1727*, was no longer able to complement the lack of chromosomal *murT-gatD* expression, since it could not reestablish the β-lactam resistance phenotype (Fig. 1A) or the growth rate (Fig. 1B). These results suggest that DUF1727 is essential for the enzymatic activity of MurT-GatD in *S. aureus*.

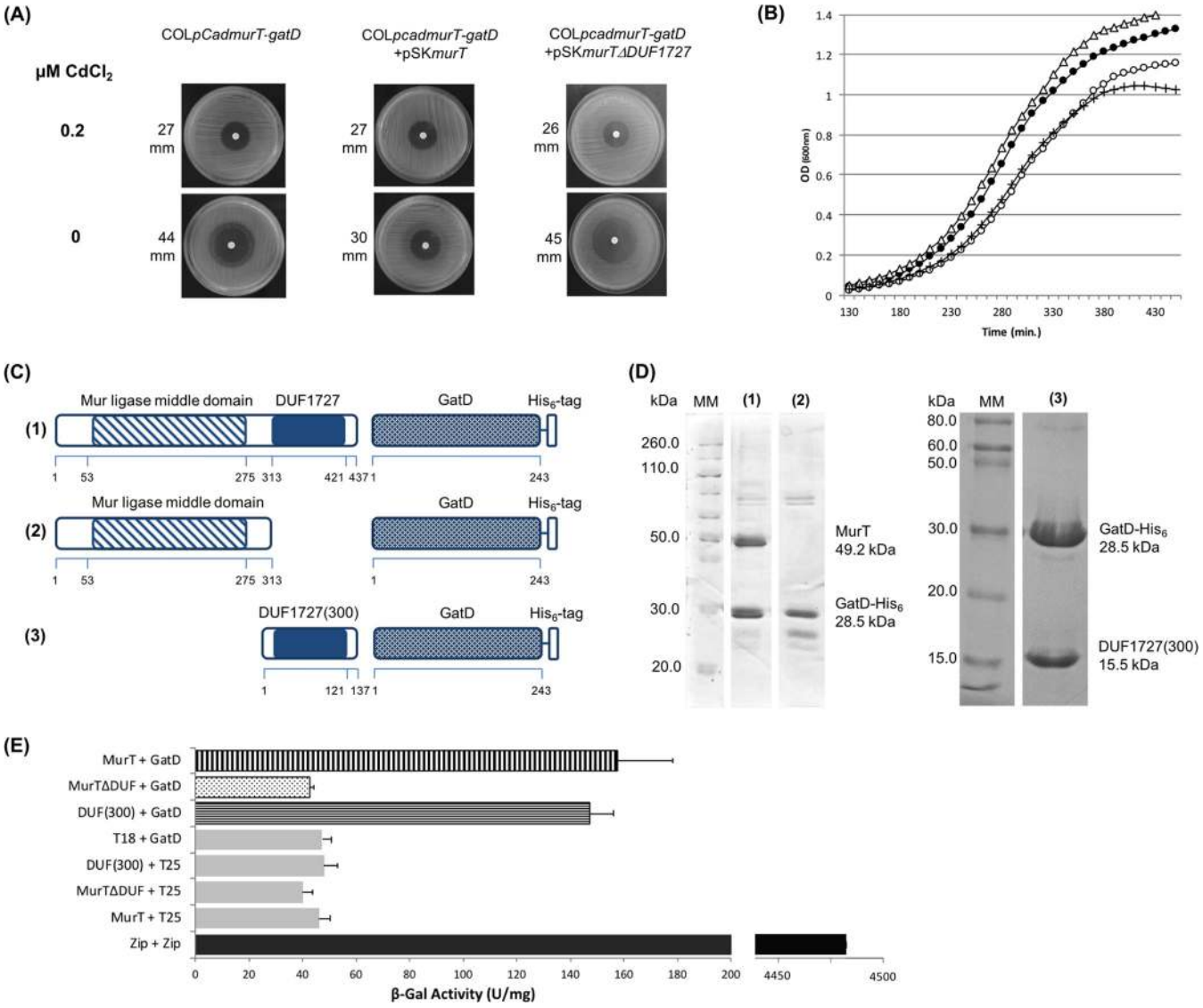

FIG 1 Role of DUF1727 in the *S. aureus* amidation phenotypes and in the MurT-GatD association. (A) Oxacillin (1 mg) growth inhibition halos for the conditional mutant COL*pCadmurT-gatD* and its complemented strains harboring the pSK*murT* or pSK*murTΔDUF1727* plasmid in the absence and presence of 0.2 μM $CdCl_2$. In the absence of inducer, the diameter of the inhibition halo was maximum (44 mm), and with 0.2 μM $CdCl_2$, the inhibition halo diameter returned to the value for parental strain COL (27 mm). The inhibition halo of COL*pCadmurT-gatD*/pSK*murT* in the absence of inducer (30 mm) results from the expression of the *murT* gene, provided in *trans*, which partially complements the lack of *murT-gatD* chromosomal expression. With the inducer, the inhibition halo diameter returned to the value for the parental strain. (B) Growth profiles of parental strain COL (Δ), conditional mutant COL*pCadmurT-gatD* (○), and complemented strains harboring the pSK*murT* plasmid (●) or the pSK*murTΔDUF1727* plasmid (+); all strains were grown without the inducer. (C and D) Schematic representations of the protein complex derivatives (C) constructed and analyzed by coelution assays in which the elution fractions of the MurT-GatD-His_6 coexpression systems were analyzed by SDS-PAGE (D). (Left) Twelve percent polyacrylamide (lane 1, MurT-GatD-His_6; lane 2, MurTΔDUF-GatD-His_6); (right) 20% polyacrylamide [lane 3, DUF1727(300)-GatD-His_6]. MM, molecular markers. (E) MurT-GatD interactions assayed by use of a BACTH system determining the β-galactosidase (β-Gal) activity of cotransformants. Negative controls included one fusion of the proteins under test and the counterpart partner domain, T18 or T25 (gray bars). A positive control for the BATCH system (Zip-Zip interaction) was used. The associated standard deviations are shown.

Role of DUF1727 in the formation of the MurT-GatD complex. The *murT-gatD* operon of *S. aureus* was cloned into plasmid pET28a, resulting in a coexpression system, pET28a*murT-gatD*, in which the MurT protein has no tag and GatD includes a C-terminal His_6 tag (Fig. 1C, row 1). Purification assays showed that MurT (49.2 kDa) coeluted with the GatD-His_6 tag protein (28.5 kDa) from an immobilized-metal affinity chromatography (IMAC) column in a 1:1 ratio, as previously described (8), demonstrating that MurT and GatD interact with a high affinity (Fig. 1D, lane 1).

The pET28a*murT-gatD* genetic construct was used to test the role of DUF1727 as the physical link between MurT and GatD. As before, the L313 residue of the MurT protein

was replaced by a stop codon, generating plasmid pET28a*murTΔDUF1727-gatD*, which yields a truncated MurT protein without the DUF1727 C-terminal domain (Fig. 1C, row 2). This truncation resulted in the complete lack of coelution of the MurT central domain (expected molecular mass, approximately 35 kDa) with GatD (Fig. 1D, lane 2, and Fig. S1C, top), suggesting that the MurT-GatD interaction occurs through DUF1727.

To test this hypothesis, two coexpression systems, pET28a*DUF1727(300)-gatD* and pET28a*DUF1727(313)-gatD* were constructed. In these systems, the DUF1727(300) and DUF1727(313) proteins (Fig. 1C, row 3, and Fig. S1B) were coexpressed with the GatD-His_6 tag. The purification procedure showed that proteins with predicted molecular masses of approximately 13.8 kDa and 15.5 kDa coeluted together with the GatD-His_6 tag protein from the IMAC column (Fig. 1D, lane 3, and Fig. S1C, bottom, lanes 6 and 7). The corresponding bands were excised from the SDS-PAGE gel and analyzed by mass spectrometry (MS), confirming that the bands corresponded to the DUF1727 proteins (Fig. S1D). The DUF1727(300) protein was selected for continued use in the study due to its higher thermal stability, as determined by differential scanning fluorimetry (Thermofluor) analysis (Fig. S1E).

These results show that the DUF1727 domain is, by itself, able to interact with the GatD protein in the absence of the central domain of MurT, suggesting that DUF1727 is responsible for the association of the two members of the enzymatic complex.

To confirm the results of the affinity pulldown assays, an *in vivo* bacterial adenylate cyclase two-hybrid (BACTH) system was used (14) under conditions that closely mimic the native environment of the complex. The three combinations of a T25-*gatD* fusion and a T18-*murT*-derived fusion [*murT*, *murTΔDUF1727*, and *DUF1727(300)*] and the four combinations of a fusion vector and an empty vector (as negative controls) were tested. β-Galactosidase activity was determined for the pUT18C*murT*/pKT25*gatD* and pUT18C*DUF1727(300)*/pKT25*gatD* cotransformants that showed comparable β-galactosidase activity values (approximately 150 U/mg), while the pUT18C*murTΔDUF1727*/pKT25*gatD* cotransformant showed β-galactosidase activity of less than 50 U/mg, a value similar to that for the negative-control cotransformants, pUT18C/pKT25*gatD*, pUT18C*DUF1727(300)*/pKT25, pUT18C*murTΔDUF1727*/pKT25, and pUT18C*murT*/pKT25. The leucine-zipper domain (Zip+Zip) was used as a positive control (Fig. 1E).

These results agreed with those of the pulldown assays, confirming that the DUF1727 domain is responsible for the interaction between MurT and GatD (Fig. 1D, lanes 2 and 3).

Identification of conserved regions of the DUF1727 domain. The alignment of MurT amino acid sequences (Fig. 2A) belonging to different Gram-positive bacterial and archaeal species representative of different taxa (Table S3) was performed with the ClustalW algorithm. Through this analysis, four regions of conserved amino acid sequence were identified in DUF1727 and designated region I (residues I311 to G319), region II (residues L340 to D355), region III (residues G373 to A386), and region IV (residues I415 to L421) (highlighted in yellow, blue, green, and red, respectively, in Fig. 2). These conserved regions are highlighted in the three-dimensional structure (Fig. 2B) with the corresponding colors. Structural analysis shows that the four regions of sequence conservation, although they are evenly distributed along the DUF1727 sequence, colocalize on the DUF1727 structure (Fig. 2B). From these observations, we hypothesized that these regions are involved in the MurT and GatD interaction and are important for the activity of the enzymatic complex.

Of the 46 residues that constitute the four conserved regions, 11 were chosen (highlighted with arrows) for further analysis (Fig. 2A). The choice was based on at least one of the following criteria: (i) the degree of conservation of the residues, (ii) the frequency of their occurrence as hot spots (15), and (iii) the surface exposure of their side chains according to the structural analysis. These 11 residues, L313, P317, D346, D349, W352, Y354, D355, R375, L381, L385, and Y418, indicated in Fig. 2, were independently altered to alanine.

Impact of substitution of DUF1727 conserved amino acids on MurT-GatD interaction. To determine if amino acid alterations would result in a decrease in

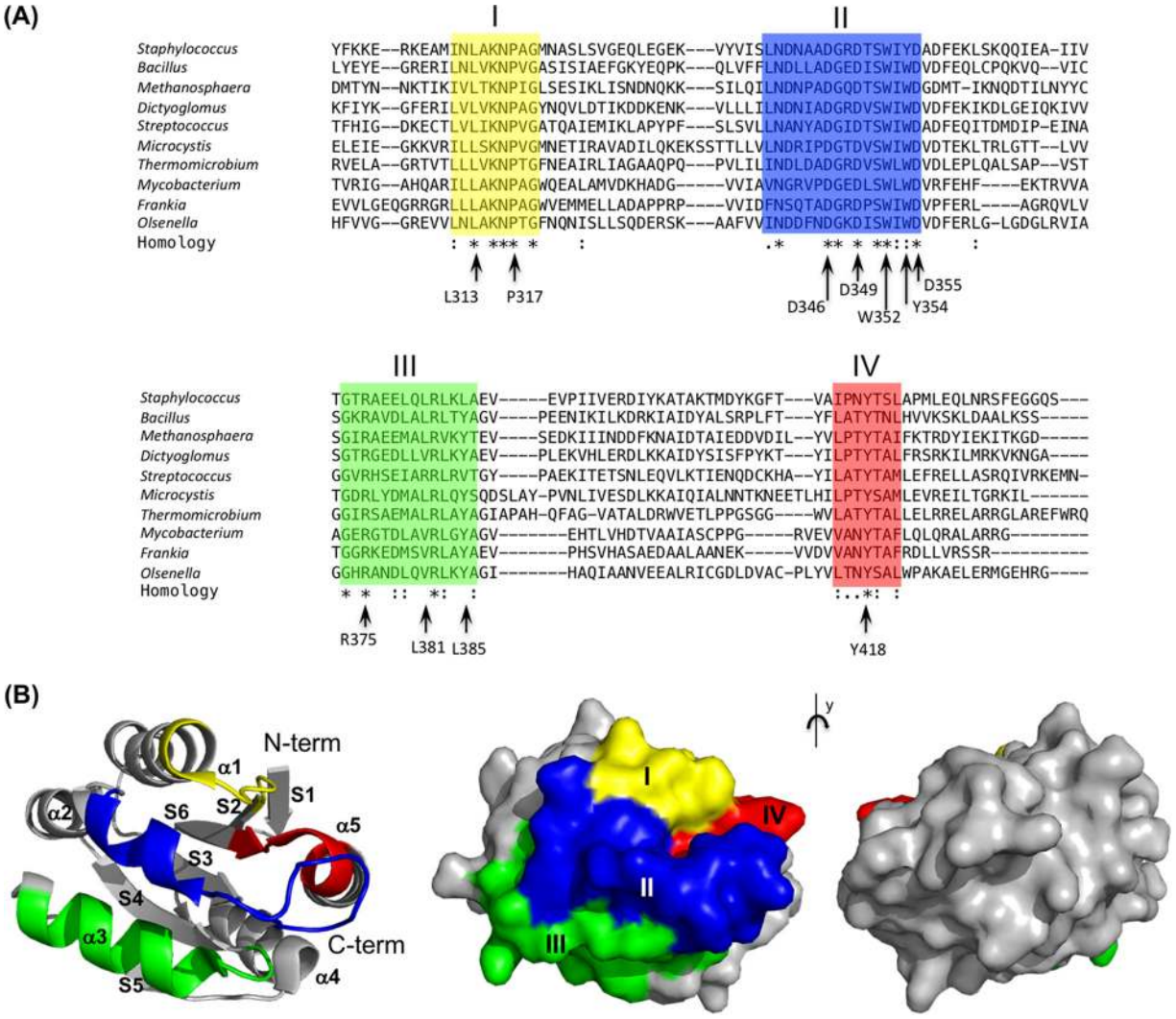

FIG 2 (A) Amino acid sequence alignment of the DUF1727 domains of 10 phylogenetically distant bacterial species, *Staphylococcus aureus* COL, *Bacillus cereus* BDRD ST196, *Methanosphaera stadtmanae* ATCC 43021, *Dictyoglomus thermophilum* ATCC 35947, *Streptococcus pneumoniae* TIGR4, *Microcystis aeruginosa* NIES-843, *Thermomicrobium roseum* ATCC 27502, *Mycobacterium tuberculosis* KZN1435, *Frankia alni* ACN14a, *Olsenella uli* ATCC 49627, performed using the ClustalW algorithm. Four regions with high sequence conservation were identified and are highlighted: region I (yellow), region II (blue), region III (green), and region IV (red). The arrows in the sequences indicate the amino acid residues chosen for alanine substitution assays. (B) Structure of DUF1727 from *S. aureus* (PDB accession number 6GS2). The conserved regions I, II, III, and IV are highlighted with the corresponding colors described in the legend to panel A and cluster on one side of the structure of the domain (as seen by the lack of color on the opposite surface of the rotated structure; right). An asterisk (*) indicates positions which have a single, fully conserved residue. A colon (:) indicates that one of the following strong groups is fully conserved: STA, NEQK, NHQK, NDEQ, QHRK, MILV, MILF, HY, FYW. A period (.) indicates that one of the following weaker groups is fully conserved: CSA, ATV, SAG, STNK, STPA, SGND, SNDEQK, NDEQHK, NEQHRK, FVLIM, HFY.

protein stability, 11 residues were replaced, performed by using the DUF1727(300) recombinant protein. This analysis could not be performed with the MurT-GatD coexpression system since some of the mutations are expected to interfere with the MurT-GatD interaction, nor could it be performed with our MurT protein expression system since it yields a protein with low solubility and poor stability.

The thermostability of each modified DUF1727(300) domain was determined by differential scanning fluorimetry, and the respective Boltzmann melting temperature (T_m) (16) was calculated when possible. The modified proteins with the P317A, R375A, L381A, L385A, and Y418A substitutions were stable and had a T_m similar to the one of the DUF1727(300) domain (Fig. S2A and B). It was not possible to calculate a T_m value for the proteins with the L313A, W352A, Y354A, and D355A substitutions (Fig. S2B), but by circular dichroism (CD) assays, these proteins were shown to be folded (Fig. S2C). The D346A and D349A substitutions showed a thermostability profile characteristic of

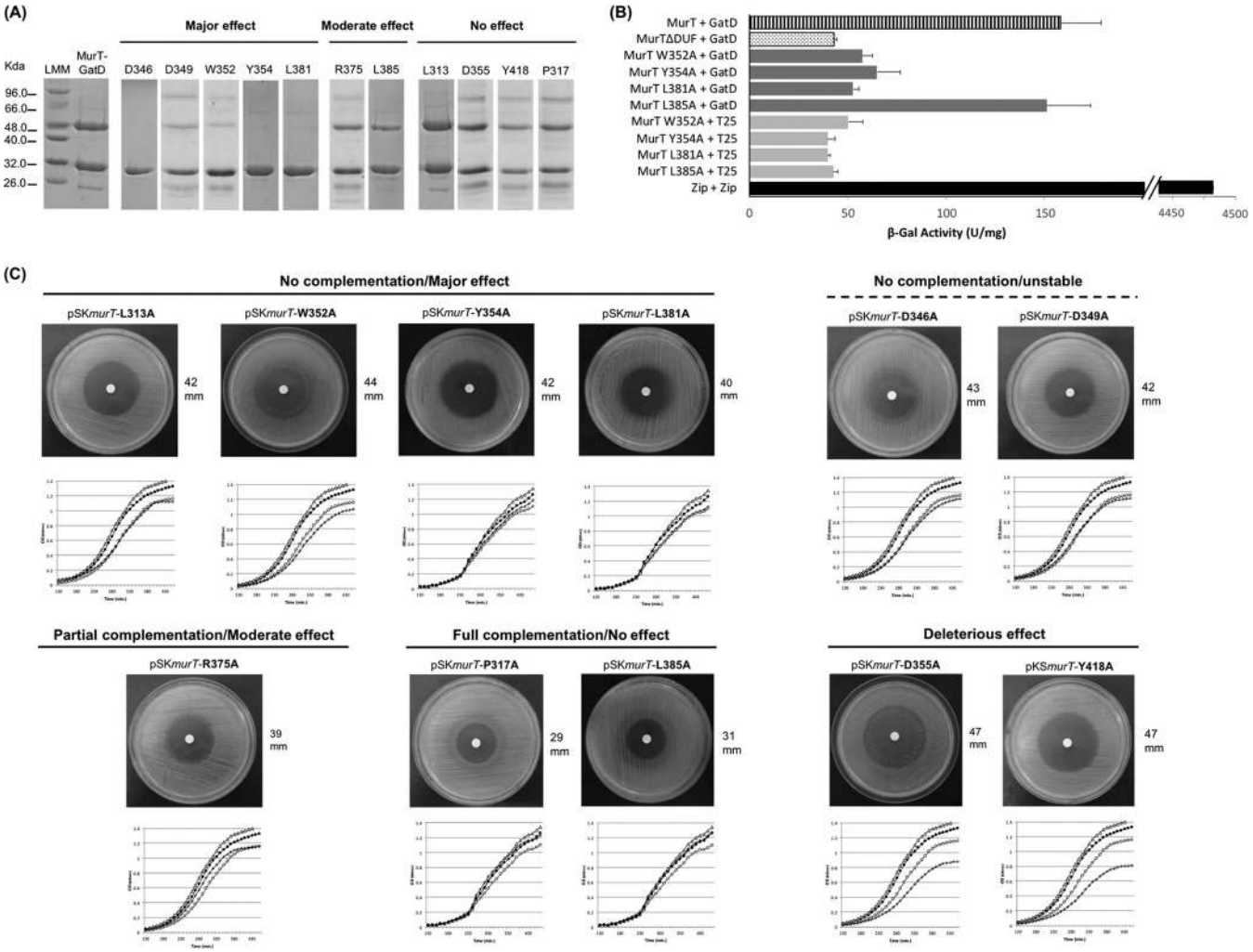

FIG 3 Protein interaction and amidation phenotypes of modified MurT-GatD systems. (A) Analysis of coelution from an IMAC column of MurT-GatD-His$_6$ proteins with different substitutions. The proteins are grouped according to the impact of complex formation. LMM, low molecular marker. (B) Impact of amino acid substitutions on the MurT-GatD interaction, determined using the bacterial two-hybrid system. Protein interactions were determined by the β-galactosidase activity of the cotransformants. Negative controls were performed using the T18C-MurT fusion proteins under test and the partner domain, T25 (light gray bars). A positive control for the BATCH system (Zip-Zip interaction) was used. (C) Oxacillin inhibition halos and growth profiles of the parental strain COL (Δ), the conditional mutant COL*pCadmurT-gatD* (○), and its isogenic complemented strains harboring the pSK*murT* plasmid (●) or the pSK*murT*-resA plasmid (+) in which "res" stands for the substituted residue. All strains were grown in the absence of the inducer.

an unfolded polypeptide, and the proteins with the substitutions were considered unstable.

The 11 residues were replaced in the MurT-GatD-His$_6$ coexpression system in order to assess the role of these conserved amino acids of DUF1727 on MurT-GatD complex formation, using the affinity pulldown approach.

Three different types of coelution profiles were obtained (Fig. 3A). (i) The first type was no coelution of the MurT protein together with GatD-His$_6$. This profile was obtained for amino acid substitutions W352A, Y354A, and L381A, in addition to the D346A and D349A modifications, which yielded unstable proteins, indicating that these amino acid substitutions have a major effect on the MurT-GatD interaction. (ii) Coelution of the MurT protein with GatD-His$_6$ in a proportion lower than 1:1 was the second type of coelution profile. This profile was obtained for the R375A and L385A substitutions, indicating that these amino acid substitutions have a moderate effect on the MurT-GatD interaction. (iii) The final type of coelution profile was full coelution of the MurT protein with GatD-His$_6$ in a 1:1 proportion. This profile was obtained for the proteins with the L313A, P317A, D355A, and Y418A substitutions, indicating that these amino acid substitutions have no effect on the MurT-GatD interaction.

The results of the affinity pulldown assays were confirmed using the *in vivo* BACTH system for the residues shown to have a major or moderate impact on the MurT-GatD interaction. The four combinations of a *gatD* fusion and a *murT*-derived fusion (*murTW352A*, *murTY354A*, *murTL381A*, *murTL385A*) and the five combinations of a fusion vector and an empty vector (negative controls) were tested by β-galactosidase-specific activity assays (Fig. 3B).

The MurTW352A-GatD, MurTY354A-GatD, and MurTL381A-GatD pairs showed a value of β-galactosidase activity similar to that for the negative controls (less than 50 U/mg). MurTL385A-GatD showed β-galactosidase activity of approximately 150 U/mg, a value similar to that for the MurT-GatD pair, suggesting that the L385A amino acid substitution does not dramatically affect the MurT-GatD interaction (Fig. 3B). The BACTH system confirmed the results from the pulldown assays, regarding the fact that amino acid residues W352, Y354, and L381 play major roles in the establishment of a physical interaction between MurT and GatD.

Among the 11 residues analyzed, W352, Y354 (region II), and L381 (region III) are necessary for the MurT-GatD association and residue R375 (region III) seems to contribute to the full association; D346 and D349 (region II) are essential for domain stability, while the other residues tested are not involved in the association (Fig. 2A and B).

Phenotypic impact of the substitution of DUF1727 conserved amino acids in *S. aureus*. To determine the impact of the conserved amino acid residues of DUF1727 on the phenotypes associated with peptidoglycan amidation in *S. aureus*, mutagenized pSK*murT* plasmids were introduced into the conditional mutant COL*pCadmurT-gatD*. The complementation profile of the strains obtained were compared with the complementation profile of COL*pCadmurT-gatD*/pSK*murT* in the absence of the inducer $CdCl_2$. Oxacillin growth inhibition halos and growth profiles were compared to test the complementation capacity of the mutagenized *murT* copy provided in *trans* (Fig. 3C). The findings were as follows. (i) Complementation by pSK*murT* was completely abolished by the substitution of residues L313, W352, Y354, and L381; the mutant strains showed 40- to 44-mm oxacillin growth inhibition halos, corresponding to no complementation; i.e., these residues are essential for the oxacillin resistance phenotype. (ii) An intermediate profile was obtained for the strain carrying pSK*murT* with mutated residue R375; the strain showed an oxacillin growth inhibition halo and a growth curve profile corresponding to partial complementation; i.e., these residues are involved in the oxacillin resistance phenotype. (iii) Complementation is not affected by the substitution of residues P317 and L385; the strains showed 29- to 31-mm oxacillin inhibition halos, corresponding to full complementation; i.e., these residues are not essential for the oxacillin resistance phenotype. (iv) The substitution of residues D346A and D349, as expected, abolished the complementation by pSK*murT*, as these mutations originate unstable polypeptides. (v) Interestingly, mutation of residues D355 and Y418 had an unexpected impact, as the presence of the respective mutated pSK*murT* plasmid negatively affected the oxacillin resistance phenotype and the growth profile; i.e., these residues showed a deleterious effect. In fact, these substitutions resulted in a more extensive decrease in the oxacillin resistance phenotype for the mutants (inhibition halo, 47 mm) than for the COL*pCadmurT-gatD* mutant grown in the absence of inducer (inhibition halo, 44 mm). The same behavior occurred for the growth rate (Fig. 3C). In the presence of inducer, the parental phenotypes were fully reestablished. In addition, more than one independent mutant clone was tested for each mutation, and each clone showed the same behavior. Substitution of these two residues did not impair the pulldown of MurT by GatD-His_6, indicating that they are not involved in the interaction between MurT and GatD, and the two residues were tested for their role in MurT-GatD enzymatic activity.

Lipid II amidation activity of altered MurT-GatD complexes. To assess the enzymatic activity of the modified forms of the MurT-GatD complex that showed

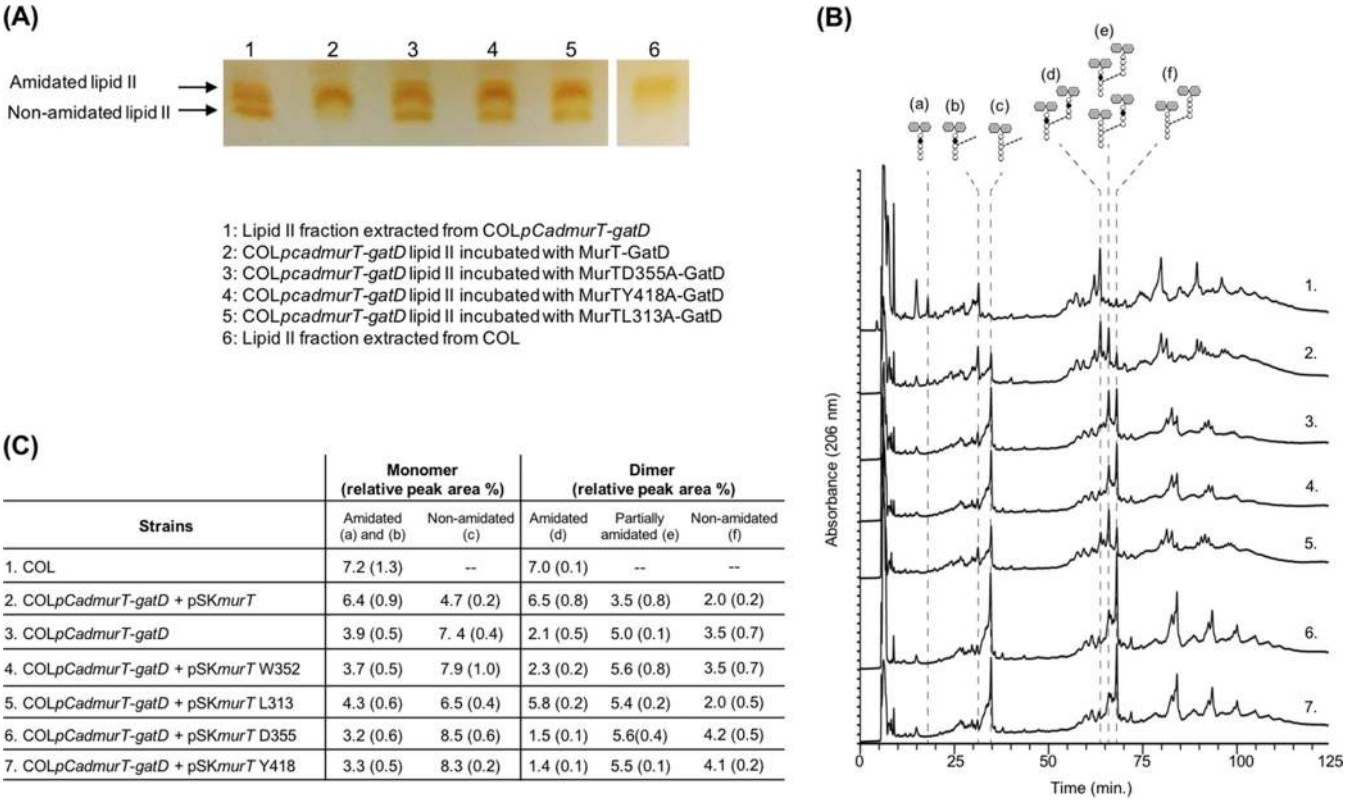

(C)

Strains	Monomer (relative peak area %)		Dimer (relative peak area %)		
	Amidated (a) and (b)	Non-amidated (c)	Amidated (d)	Partially amidated (e)	Non-amidated (f)
1. COL	7.2 (1.3)	--	7.0 (0.1)	--	--
2. COL*pCadmurT-gatD* + pSK*murT*	6.4 (0.9)	4.7 (0.2)	6.5 (0.8)	3.5 (0.8)	2.0 (0.2)
3. COL*pCadmurT-gatD*	3.9 (0.5)	7. 4 (0.4)	2.1 (0.5)	5.0 (0.1)	3.5 (0.7)
4. COL*pCadmurT-gatD* + pSK*murT* W352	3.7 (0.5)	7.9 (1.0)	2.3 (0.2)	5.6 (0.8)	3.5 (0.7)
5. COL*pCadmurT-gatD* + pSK*murT* L313	4.3 (0.6)	6.5 (0.4)	5.8 (0.2)	5.4 (0.2)	2.0 (0.5)
6. COL*pCadmurT-gatD* + pSK*murT* D355	3.2 (0.6)	8.5 (0.6)	1.5 (0.1)	5.6(0.4)	4.2 (0.5)
7. COL*pCadmurT-gatD* + pSK*murT* Y418	3.3 (0.5)	8.3 (0.2)	1.4 (0.1)	5.5 (0.1)	4.1 (0.2)

FIG 4 (A) Amidation assay of *S. aureus* lipid II analyzed by TLC. For the enzymatic reactions, COL*pCadmurT-gatD* lipid II was incubated with ATP, glutamine, and the protein complex. Lane 1, COL*pCadmurT-gatD* lipid II (2 bands corresponding to amidated and nonamidated forms); lanes 2 to 5, COL*pCadmurT-gatD* lipid II incubated with the MurT-GatD complex and MurT-GatD complexes altered in residues D355, Y418, and L313, respectively; lane 6, COL lipid II (1 band corresponding to fully amidated lipid II). (B) RP-HPLC profiles of the peptidoglycan of parental strain COL, conditional mutant COL*pCadmurT-gatD*, complemented strain COL*pCadmurT-gatD*/pSK*murT*, and the mutants complemented with copies of *murT* altered in residues W352, L313, D355, and Y418, all of which were grown in the absence of the inducer. The muropeptide structures (a, amidated monomer; b, amidated monomer with pentaglycine bridge; c, nonamidated monomer with pentaglycine bridge; d, amidated dimer; e, partially amidated dimer; f, nonamidated dimer) were identified by assessing the relative elution times, and the structures were compared to previously identified muropeptide structures by mass spectrometry. (C) The peaks of the chromatogram were integrated, and the values are presented as a percentage of the total area of the chromatogram. The values correspond to the means from three independent replicates, and the standard deviation values are in parentheses.

unpaired amidation phenotypes (L313A, D355A, Y418A), lipid II was extracted from the *S. aureus* conditional mutant COL*pCadmurT-gatD* as described previously (17).

The lipid II fraction extracted from the COL*pCadmurT-gatD* mutant shows the presence of two bands by thin-layer chromatography (TLC) which corresponds to a mixture of approximately 50% of amidated and 50% nonamidated lipid II forms (Fig. 4A, lane 1). By comparing this migration pattern with the migration pattern of the lipid II fraction of strain COL, which produced a single band corresponding to fully amidated lipid II (Fig. 4A, lane 6), the amidated lipid II form was identified as the top band in the TLC plate, while nonamidated lipid II corresponded to the bottom band, as described before (8).

Each protein complex was incubated with lipid II and with the substrates ATP and glutamine, and separation was performed by TLC. In the control amidation reaction (Fig. 4A, lane 2), the lipid II fraction extracted from the COL*pCadmurT-gatD* mutant was incubated with the wild-type (wt) MurT-GatD protein complex; one band was observed, demonstrating that the wt MurT-GatD complex could fully amidate the lipid II present. When the same lipid II extract was incubated with the MurT-GatD complex proteins with amino acid substitutions (Y418A, D355A, L313A), the two bands were always observed in approximately the same proportion. Taken together, these results show that the Y418, D355, and L313 residues of MurT DUF1727 are essential for the amidation reaction and the amidation phenotype.

Comparison of the level of peptidoglycan amidation in different *S. aureus murT-gatD* mutants. The cell walls of the parental strain COL, the conditional mutant (COL*pCadmurT-gatD*), the complemented mutant (COL*pCadmurT-gatD*/pSK*murT*), and the mutants complemented with *murT* altered copies in residues W352, L313, D355, and Y418 grown in the absence of inducer were extracted, the peptidoglycan was purified and digested with muramidase, and the muropeptides were analyzed by reverse-phase high-performance liquid chromatography (RP-HPLC) (Fig. 4B and C). We analyzed the area values of the peaks corresponding to monomeric and dimeric muropeptides, as these peaks are representative of peptidoglycan amidation and are well resolved. These structures were identified by assessing the relative elution times and comparing to previously identified muropeptide structures by mass spectrometry (18, 19).

As described previously (5), the elution profile of the conditional mutant showed higher retention times for all peaks than that of strain COL and splitting of the peaks of higher oligomerization muropeptides, due to a lack of amidation of one or more stem peptides of the oligomer (Fig. 4B, traces 1 and 3). The elution profile of the mutant complemented with pSKmurT showed partial reestablishment of the mutant muropeptide pattern, and the mutant complemented with pSKmurT had a higher percentage of amidated muropeptides than the conditional mutant (Fig. 4B, trace 2).

The peptidoglycan profile of COL*pCadmurT-gatD*/pSK*murT*W352 was very similar to that of mutant strain COL*pCadmurT-gatD* (Fig. 4B, traces 4 and 3, respectively). The mean ± standard deviation percentages of amidated muropeptides incorporated into these strains were 3.7% ± 0.5% and 3.9% ± 0.5%, respectively, for monomers and 2.3% ± 0.2%, and 2.1% ± 0.5%, respectively, for fully amidated dimers (Fig. 4C). These results show that the mutation of pSK*murT*W352 is unable to complement the conditional mutant regarding the peptidoglycan amidation level.

For COL*pCadmurT-gatD*/pSK*murT*L313, the percentage of amidated muropeptides was 4.3% ± 0.6% and 5.8% ± 0.2% for monomers and fully amidated dimers, respectively (Fig. 4B, trace 5, and Fig. 4C, row 5), showing a lower level of peptidoglycan amidation than COL*pCadmurT-gatD*/pSK*murT* (Fig. 4B, trace 2, and Fig. 4C, row 2).

The peptidoglycan profiles of COL*pCadmurT-gatD*/pSK*murT*D355 and COL*pCadmurT-gatD*/pSK*murT*Y418 were virtually indistinguishable from one another, with these two strains showing a higher degree of nonamidation than mutant strain COL*pCadmurT-gatD*. In these two strains, the percentage of amidated monomeric (3.2% ± 0.6% and 3.3% ± 0.5%, respectively) and dimeric muropeptides (1.5% ± 0.1% and 1.4% ± 0.1%, respectively) incorporated was even lower than that for the mutant strain (3.9% ± 0.5% of monomers and 2.1% ± 0.5% of dimers) (Fig. 4B).

DISCUSSION

Using two complementary approaches, the *in vitro* pulldown assay and the *in vivo* interaction assay, we established that DUF1727 is responsible for the interaction between the two proteins MurT and GatD and for complex formation. This observation was confirmed by recent crystallographic structures, where GatD docks to the C terminus of MurT (20, 21). Our results, obtained using distinct approaches, showed that DUF1727 is sufficient for the interaction with GatD and, more importantly, is essential for complex activity.

DUF1727 has four amino acid regions that are phylogenetically conserved. These four regions, although evenly distributed along the sequence, colocalize in the three-dimensional structure (Fig. 2). The functional role of these regions was addressed by targeting conserved amino acid residues by site-directed mutagenesis. The residues with an impact on the physical association of the two proteins were found to cluster in regions II and III.

Our results show that residues W352, Y354, L381, and R375 are essential for complex formation. The release of the MurT-GatD structure from *S. aureus* (PDB accession numbers 6GS2 and 6H5E) confirmed that Y354, L381, and R375 are located at the dimer interface, performing essential contacts between DUF1727 and the GatD enzyme

(A)

Amino acid	MurT-GatD association	Amidation Phenotypes	PG amidation (*)	Lipid II amidation	Dimer Interface (pdb 6gs2)
W352	Major effect	Major effect	Low	ND	No
Y354	Major effect	Major effect	ND	ND	Yes
L381	Major effect	Major effect	ND	ND	Yes
R375	Moderate effect	Moderate effect	ND	ND	Yes
L313	No effect	Major effect	Low	No amidation	No
D355	No effect	Deleterious effect	Residual	No amidation	Yes(**)
Y418	No effect	Deleterious effect	Residual	No amidation	No
L385	No effect	No effect	ND	ND	Yes
P317	No effect	No effect	ND	ND	No
D346	Major effect	Major effect	ND	ND	No
D349	Moderate effect	Major effect	ND	ND	Yes-active site

* In comparison to the conditional mutant, considered to have low levels of amidation.
** At the edge of the interface with GatD.
ND: not determined.

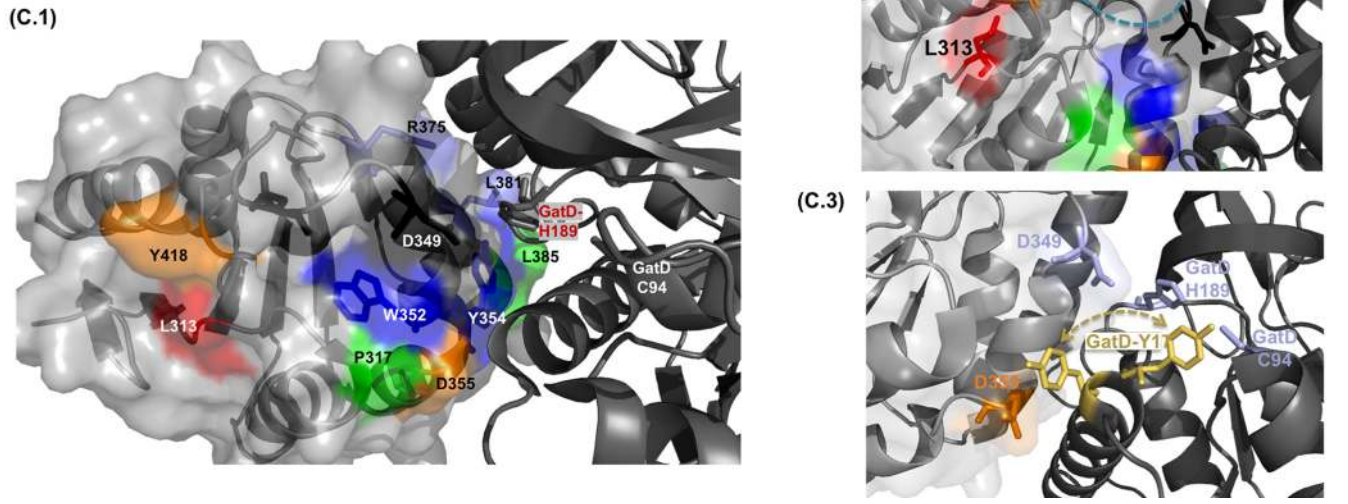

FIG 5 (A) MurT-GatD interaction, amidation phenotypes, and activity associated with each amino acid substitution. Blue, amino acids for which the mutations induced an amidation phenotype that can be associated with a loss of interaction of the enzymatic complex; red and orange, amino acids which show a major or deleterious effect, respectively, on the amidation phenotype but the proteins maintain a full association; green, residues for which mutant proteins behave like the native pair; gray, residues whose effects can be attributed to the loss of protein stability. PG, peptidoglycan. (B) Surface representation of DUF1727 structure (PDB accession number 6GS2). The conserved residues L313, P317, D346, D349, W352, Y354, D355, R375, L381, L385, and Y418 are highlighted with the corresponding colors described in the legend to panel A. (C) Structural representation of the MurT-GatD complex. MurT is shown as a ribbon representation with a light gray surface, and GatD is shown as a ribbon representation in dark black (PDB accession number 6GS2). Conserved residues are colored as described in the legend to panel A. GatD catalytic residues are identified and shown in stick representation. (C.1) The DUF1727 domain anchors to the GatD protein. Residues Y354, R375, L381, and W352 (side chains in blue) are essential for complex formation and activity. (C.2) Structural proximity of residues L313 (red) and Y418 (orange) to the DNAAD motif in the DUF1727 domain. The residues of the DNAAD motif are represented with sticks and indicated with a blue circle. (C.3) In chain A of the structure with PDB accession number 6GS2, GatD residue Tyr17 has two distinct locations, suggesting two distinct conformations. In one conformation, this residue is near MurT-D355 (orange), while in the other conformation, it is close to GatD active-site residues represented in blue (C94 and H189). This interconversion between conformations suggests a regulatory role for the GatD-Y17 residue and an essential contribution of the MurT-D355 residue.

(Fig. 5B and C.1). The crystallographic structure shows that MurT-Y354 contacts with two prolines in the GatD β13-α6 loop (P191 and P194), as MurT-L381 also contacts with GatD-P194 (21). W352 is not located on the contact surface between MurT and GatD, as the indole ring is partially buried in the DUF1727 structure (Fig. 5.C.1). As the substitution performed was to an alanine, the difference in the residue size may result in a local conformational change that interferes with other residues at the interface. The detrimental effect of the substitution of these four amino acids, W352, Y354, L381, and R375, on complex formation was in accordance with the effect on the amidation phenotypes with a lack of complementation, namely, a decrease in β-lactam resistance

and the growth rate. For W352, we also observed decreased levels of peptidoglycan amidation.

The alanine modifications of residues P317 and L385 did not affect complex formation and had no effect on the amidation phenotype (full complementation) (Fig. 5A). Substitution of L385 could be expected to prevent complex formation, since structure analysis shows that this residue is part of a hydrophobic core at the dimer interface. However, modification of L385 to alanine (a smaller hydrophobic residue) resulted in a behavior similar to that of the parental strain. A more pronounced effect might have been observed if mutation to a charged or a polar residue was done.

The recently published structures of the MurT-GatD complexes from *S. pneumoniae* and *S. aureus* revealed a unique role for the C-terminal domain of MurT (DUF1727). Residue D349 plays a pivotal role in glutaminase activity by completing the catalytic triad (21). Our MurT-D349A mutation was responsible for a loss of complex formation and was not able to complement the amidation phenotype, which we attribute to the loss of protein stability and, consequently, its function (Fig. 5A).

More importantly, we identified residues L313, D355, and Y418 on DUF1727 to be essential for lipid II amidation *in vitro* and peptidoglycan amidation *in vivo*, with resulting consequences in the phenotypic assays (no complementation or deleterious effect), although they did not affect formation of the complex (Fig. 5A). These results demonstrate that DUF1727 has other essential roles in the enzymatic activity of the complex, in addition to completing the GatD catalytic triad.

In the Mur ligase family, the C-terminal domain is involved in orienting the incoming amino acid (substrate) into its active site. The DUF1727 domain has the same fold topology as the C-terminal domains of the Mur ligases, although they have no sequence similarity (see Fig. S3 in the supplemental material). By analogy to its structural homologs, DUF1727 could act as a channel for ammonia from the GatD catalytic site to the MurT active site, directing it closer to the other substrate, the lipid-linked peptidoglycan precursor.

Residues L313 and Y418 are in close proximity to the DNAAD motif (residues 342 to 346) of MurT previously identified to be essential for substrate recognition (Fig. 5C.2) (8). The corresponding motif (DDPR) of the MurE protein of *Thermotoga maritima* (22) was shown to recognize the incoming lysine and incorporate it into the UDP-MurNAc dipeptide. In the crystal structure of MurE from an meso-diaminopimelic acid (mDAP)-dependent *E. coli* strain, all the residues in the DNPR motif were shown to be involved in mDAP substrate binding (23). In the crystal structure of MurE from *S. aureus* bound to its UDP-MurNAc tripeptide product, the ε-amino group of the L-lysine residue of the UDP-MurNAc tripeptide was bound to the MurE D406 residue, the first aspartate of the DNPA motif, in concert with E460 (24).

Due to their structural proximity to the DNAAD motif (Fig. 5C.2), it is proposed that residues Y418 and L313 of the DUF1727 domain are involved in the recognition and channeling of the ammonia from glutamine hydrolysis at the active site to the ATP binding motif of MurT. This hypothesis accounts for the essential role of these two highly conserved residues in the amidation phenotype in *S. aureus*.

Modification of residue D355 impairs the enzymatic activity, decreases peptidoglycan amidation, and has a deleterious effect on the amidation phenotypes. Combined, these results show that this residue has a pivotal role in the catalytic mechanism of the complex. The active site of GatD includes C94, H128, and MurT-D349 (21, 25), and it has been shown that residues Y17 and R128 of GatD are important in blocking the substrate path to the active site, having a regulatory role in glutaminase activity (25). In the MurT-GatD structure from *S. aureus*, the GatD-Y17 residue can adopt two distinct conformations. This observation is clearly demonstrated by the structure with PDB accession number 6GS2 chain A, where GatD-Y17 can be positioned toward DUF1727 or in close proximity to H189 and C94 at the GatD active site with roughly 50% occupancy for both states in the crystal (Fig. 5C.3). The dynamic property of this region of GatD might have an important regulatory role. When facing DUF1727, GatD-Y17 is close to MurT-D355 (Fig. 5C.3). In this conformation, the hydroxyl group of GatD-Y17

can form a hydrogen bond with the carboxyl group of MurT-D355. This interaction must be important for the catalytic mechanism of the complex, as substitution of D355 for alanine has a deleterious effect in *S. aureus*.

Our results show that DUF1727 is responsible for the physical link between MurT and GatD. More importantly, DUF1727 has other essential roles in the activity of the complex. DUF1727 is proposed to recognize and channel the ammonia group produced by the GatD partner through the DNAAD motif and residues L313 and Y418 (Fig. 5C.2). In addition, D355 is involved in regulating the glutaminase activity, interacting with GatD-Y17, involved in substrate access to the GatD active site.

Inhibiting the activity of MurT-GatD would be a specific approach against Gram-positive pathogens. Blocking the association between MurT and GatD or the activity of the complex by targeting the C-terminal domain of MurT should provide a novel way to therapeutically interfere with bacterial cell wall synthesis. Our results have allowed us to identify residues that can be used to develop a pharmacophoric template to design small-molecule inhibitors of MurT-GatD and thus boost bacterial susceptibility to lysozyme and β-lactam antibiotics.

As the acquisition of resistance is a major constraint to the efficacy of treatment of multiresistant infections, the development of a combined therapy using drugs that would resensitize the pathogen to β-lactams and the host immune system is a promising strategy to pursue in the future.

MATERIALS AND METHODS

Bacterial strains, plasmids, and growth conditions. The bacterial strains and plasmids used in this study are listed in Table S1 in the supplemental material. *Escherichia coli* strains were grown at 37°C in lysogeny broth (LB; NZYTech, Portugal) or in LB agar (LA; NZYTech) in the presence of the respective antibiotics (Table S1): ampicillin (Amp) at 100 μg/ml, kanamycin (Km) at 30 μg/ml (for manipulation of strains carrying pET28a and derivatives) or 50 μg/ml (for BACTH assays), and chloramphenicol (Cm) at 50 μg/ml (Sigma, St. Louis, MO). The *S. aureus* strains were grown in tryptic soy broth (TSB; Difco Laboratories, USA) or in tryptic soy agar (TSA; Difco Laboratories) at 37°C in the presence of Km at 50 μg/ml, neomycin (Neo) at 50 μg/ml (Sigma), and Cm at 10 μg/ml, when appropriate (Table S1). The growth medium of the *S. aureus* conditional mutant was supplemented with 0.2 μM cadmium chloride ($CdCl_2$; Sigma), unless otherwise indicated. Growth in liquid medium was monitored by measuring the optical density at 600 nm (OD_{600}) of the cultures.

DNA general methods. Restriction enzymes from Thermo Scientific (Waltham, MA, USA) were used as recommended by the manufacturer. Routine PCR amplification was performed with NZYTaq DNA polymerase (NZYTech), and PCR amplification for cloning and site-directed mutagenesis purposes was performed using Phusion High-Fidelity DNA polymerase (Thermo Scientific). For plasmid DNA extraction, a ZR plasmid miniprep classic kit (Zymo Research, CA, USA) was used. PCR and digestion products were purified using NZYGelpure (NZYTech) or nitrocellulose membrane filters (MilliporeSigma, Canada).

Determination of *S. aureus* oxacillin resistance. Overnight cultures of strains COL and COL*pCad-murTgatD* and the complemented derivatives, grown with the appropriate inducer concentration, were plated on TSA and TSA supplemented with 0.2 μM $CdCl_2$ and incubated at 37°C for 48 h. Oxacillin (Sigma) diffusion disks (1 mg) were used to determine the growth inhibition halos after 24 and 48 h of incubation.

Construction of MurT-GatD protein coexpression system. The DNA fragments encompassing *murT-gatD*, DUF1727(300)-*gatD*, and DUF1727(313)-*gatD* were amplified from the *S. aureus* COL genome using primer pairs PMurT-Fw and PGatD-RV, P13aaDUF-His and PGatD-RV, and PDUF-His and PGatD-RV, respectively (Table S2). DNA fragments were cloned into the pET28a vector using the NcoI and XhoI restriction sites to generate a C-terminal GatD-His_6 fusion protein. Ligation reactions were performed using T4 DNA ligase (NZYTech). The *E. coli* DH5α host was transformed with the ligation mixture, and positive transformants were screened by PCR and sequenced. The correct recombinant plasmids were designated pET28a-*murT-gatD*-His_6, pET28a-*DUF(300)-gatD*-His_6, and pET28a-*DUF(313)-gatD*-His_6.

Plasmid pET28a-*murT-gatD*-His_6 was used as the DNA template to generate the plasmid expressing MurT without the DUF1727 C-terminal domain and GatD-His_6 by SDM. The second thymine nucleotide of the codon (TTA), which codes for Leu313, of the DUF1727 domain was replaced by a guanine nucleotide, producing a stop codon (TGA), thus blocking the translation of the C-terminal domain of MurT. The plasmids were used to transform *E. coli* DH5α competent cells, and after confirmation of the site-directed mutant by sequencing, the plasmids were transferred into the expression strain *E. coli* BL21(DE3).

Construction of DUF1727 recombinant domains. The DNA fragments *DUF1727(313)*, *DUF1727(300)*, *DUF1727(275)*, and *DUF1727(191)* were amplified from the *S. aureus* COL genome using the primer pairs described in Table S2. The DNA fragments were cloned into the pET28a vector using the NdeI and NotI restriction sites to generate an N-terminal fusion protein and using the NcoI and SalI restriction sites to generate a C-terminal fusion protein. Ligation reactions and transformation were performed as described above. The correct recombinant plasmids were designated pET28a-*His_6-DUF(300)*, pET28a-*His_6-DUF(313)*, pET28a-*His_6-DUF(275)*, pET28a-*His_6-DUF(191)*, pET28a-*DUF(300)-His_6*, pET28a-*DUF(313)-His_6*,

pET28a-*DUF(275)-His$_6$*, and pET28a-*DUF(191)-His$_6$*. The plasmids were transferred into the expression strain *E. coli* Rosetta(DE3).

Overexpression and purification of recombinant proteins. For expression of DUF1727 recombinant proteins and coexpression of MurT-GatD systems, *E. coli* BL21(DE3) and *E. coli* Rosetta(DE3) cultures were incubated at 37°C with aeration until an OD_{600} of 0.6 was reached. Isopropyl-β-D-1-thiogalactopyranoside (IPTG) was added at a final concentration of 1 mM, and the culture was incubated for an additional 3 h at 30°C or 4 h at 25°C. Cells were harvested by centrifugation and resuspended in lysis buffer (20 mM Tris-HCl, pH 7.5, 500 mM NaCl) with 1 mM phenylmethylsulfonyl fluoride (PMSF) and 10 μg/ml of DNase I. The cells were sonicated (80% amplitude, 0.5 cycle, 10 times for 1 min each time) (UP100H compact ultrasonic laboratory device; Hielscher Ultrasound Technology), and the lysate was clarified by centrifugation (1 h, 4°C, 12,000 $\times$ *g*).

Purification was performed using an immobilized metal affinity column (Nacherey-Nagel, Duren, Germany). In the case of DUF1727 recombinant proteins, after IMAC a buffer exchange step to 20 mM Tris, pH 7.5, 200 mM NaCl using a PD-10 column (GE Healthcare, IL, USA) was done, and the proteins were concentrated with Amicon Ultra-15 (10,000 nominal molecular weight limit) centrifugal filter units (MilliporeSigma). The protein concentration was determined by the bicinchoninic acid method using a bovine serum albumin (BSA) protein assay reagent (Thermo Scientific). The purity of the eluted recombinant proteins was verified by SDS-PAGE analysis. The proteins were stored in 20 mM Tris, pH 8.2, 1 M NaCl, 10% glycerol at −20°C.

Mass spectrometry analysis. The protein bands of interest stained with Coomassie blue were destained, reduced, alkylated, and digested with trypsin (10 ng/μl; Promega) overnight at 37°C. The tryptic peptides were extracted, desalted, and concentrated using a Poros C_{18} column (Empore; 3M) and eluted directly onto the matrix-assisted laser desorption ionization (MALDI) plate. The data were acquired in positive-reflector MS and MS/MS modes using a 5800 MALDI-time of flight (TOF)/TOF (AB Sciex) mass spectrometer and using TOF/TOF Series Explorer software (v.4.1.0; Applied Biosystems). External calibration was performed using a CalMix5 standard (Protea). The 25 most intense precursor ions from the MS spectra were selected for MS/MS analysis.

The raw MS and MS/MS data were analyzed using Protein Pilot software (v.4.5; AB Sciex) with the Mascot search engine (MOWSE algorithm). The search was performed against the UniProt protein sequence database with a taxonomy restriction to *Staphylococcus aureus* and *Escherichia coli*. A maximum of two missed cleavages was allowed. Protein identification was accepted only when significant protein homology scores were obtained ($P < 0.05$) and at least one peptide was fragmented with a significant individual ion score ($P < 0.05$). The MS data were provided/obtained by the Mass Spectrometry Unit (UniMS), ITQB/iBET, Oeiras, Portugal.

Identification of conserved regions of DUF1727. Alignment of the MurT amino acid sequences of 10 phylogenetically distant species (Table S3) was performed using the ClustalW program (26).

Site-directed mutagenesis. Plasmids pET28a-*murT-gatD-His$_6$*, pET28a-*DUF(300)-His$_6$*, and pSK*murT* were used as the templates for PCR amplification using *Phusion* DNA polymerase, mutagenesis primers designed to include the appropriate nucleotide substitutions (Table S2), and with the following conditions: 98°C for 1 min 30 s; 30 cycles each consisting of 98°C for 10 s, 60 to 80°C for 45 s, and 72°C for 5 to 7 min; and one final extension step of 72°C for 12 min. The PCR products were treated with DnpI (10 U) from New England Biolabs (Beverly, MA) at 37°C from 4 h to overnight to digest the parental plasmid DNA. After heat inactivation, the samples were dialyzed using nitrocellulose membrane filters (MilliporeSigma) and transformed into *E. coli* DH5α competent cells. Positive clones were confirmed by sequencing (Stabvida, Caparica, Portugal); the corresponding pET28a-derived plasmids were transformed into the *E. coli* expression strains (Table S1), and the pSK*murT*-derived plasmids were electroporated into RN4220 electrocompetent cells using a Gene Pulser apparatus (Bio-Rad, CA, USA) as described previously (29) and subsequently transduced into the COL*pCadmurT-gatD* mutant strain using phage 80α (27).

Protein stability by fluorescence thermal shift assay. Protein solutions (5 μM) were prepared in 20 mM Tris, pH 7.5, and SYPRO Orange (Sigma) was added to a final concentration of 20×; the samples were analyzed on 96-well thin-wall PCR plates (Applied Biosystems, MA, USA). Samples with no protein added or unfolded (boiled) protein were used as controls. The plates were sealed with optical adhesive film (Applied Biosystems) and submitted to a temperature gradient from 20 to 95°C in increments of 2.2°C/s using a StepOnePlus real-time PCR system (Applied Biosystems). Fluorescence alterations were monitored simultaneously with a charge-coupled-device (CCD) camera. The wavelengths for excitation and emission were 470 and 570 nm, respectively. The Boltzmann melting temperature (16) of each protein tested was calculated using Protein Thermal Shift software (v.1.3; Applied Biosystems). Three technical replicates were performed for all samples.

CD assays. Circular dichroism (CD) spectroscopy experiments were performed on a Chirascan qCD spectrometer (Applied Photophysics) under a constant nitrogen flush; the spectrometer was equipped with a temperature control system (model TC125; Quantum Northwest). The concentrations of the proteins tested were set to 0.1 mg/ml in 20 mM Tris, pH 7.5. The resulting spectra were obtained at 1-nm intervals at 20°C using a cuvette with a path length of 1 mm, and three spectral scans with an integration time of 3 s per nm were averaged.

Bacterial two-hybrid interaction assays. A bacterial adenylate cyclase two-hybrid (BACTH) system (Euromedex) was used (14). The *murT* and *gatD* genes, *murT*ΔDUF, and the *DUF1727(300)* DNA fragments were amplified using the primers listed in Table S2 and cloned into the pUT18C, pUT18, pKNT25, and pKT25 vectors in frame with two gene fragments of the adenylate cyclase of *Bordetella pertussis*. Nucleotide substitutions in the *murT* gene (L381A, L385A, W352A, and Y354A) were performed by

site-directed mutagenesis in the pUT18C-*murT* vector using the primers listed in Table S2. All cloned fragments were sequenced.

All combinations of the constructed plasmids (T18 and T25) were cotransformed into the host strain *E. coli* BTH101 (*cya*). Cotransformants were selected on LA plates supplemented with Amp (100 μg/ml) and Km (50 μg/ml) and grown at 30°C, and three colonies were isolated for further experiments to exclude clone-by-clone variation. As a positive control, strain BTH101 was cotransformed with plasmids pUT18C-zip and pKT25-zip, encoding two leucine zipper domains. As negative controls, all plasmids constructed were cotransformed with the empty plasmid carrying the partner domain of adenylate cyclase.

β-Galactosidase activity was determined colorimetrically by monitoring the cleavage of *ortho*-nitrophenyl-β-galactoside (ONPG; Thermo Scientific) into *ortho*-nitrophenol, as described by the manufacturer (Euromedex). Briefly, the cotransformants were grown overnight in LB with 500 μM IPTG and the appropriate antibiotics at 30°C and with vigorous agitation. The cultures were diluted (1:5) in M63 minimal medium, and the optical density at 600 nm of each culture was determined.

Bacterial cells were permeabilized using toluene and 0.1% SDS. The culture was vortexed, the toluene was allowed to evaporate, and the cellular suspension was vigorously agitated at 37°C for 30 min. Fresh PM2 buffer (70 mM Na_2HPO_4, 30 mM NaH_2PO_4, 1 mM $MgSO_4$, 0.2 mM $MnSO_4$, pH 7.0, 100 mM β-mercaptoethanol) was added to aliquots of the permeabilized cells to a final volume of 1 ml. The samples were incubated at 28°C for 5 min, and the reaction began upon addition of 0.25 ml of ONPG substrate solution (0.4% in PM2 buffer without β-mercaptoethanol). The reaction was stopped with 1 M Na_2CO_3 solution. After centrifugation, the OD_{420} and OD_{600} values of the supernatants were determined. For samples with OD_{420} values lower than 0.3, a correction factor was used ($OD_{420} = OD_{420} - 1.5 \times OD_{600}$) to compensate for the debris light scattering. The enzymatic activity (*A*; in units per milligram) of each sample was calculated according to the formula $A = 200 \times [(OD_{420} - OD_{420}$ for the control sample)/minutes of incubation] $\times$ dilution factor.

The result was then converted to units per milligram of cell dry weight according to the initial OD_{600} of the culture, considering that 1 ml of culture at an OD_{600} of 1 corresponds to 300 μg of cell dry weight.

The assay was performed in triplicate using independent cotransformants, and each assay included two technical replicates.

Extraction of amidated and nonamidated lipid II. Overnight cultures of *S. aureus* COL and COL*pCadmurT-gatD* were washed thrice in TSB to remove the inducer and were used to inoculate 2 liters of fresh medium supplemented with the appropriate antibiotics. At an OD_{620} of 0.6, moenomycin was added (6 μg/ml) to the culture to accumulate lipid II, and growth was allowed for a further 20 min. The extraction of lipid II was performed as previously described (17).

***In vitro* synthesis of amidated lipid II.** Lipid II was incubated with 160 mM Tris-HCl, 0.7% Triton X-100, 5 mM KCl, 40 mM $MgCl_2$, pH 7.5, 6 mM ATP, 7 mM L-glutamine for 4 h at 30°C and with 2 μg of MurT-GatD purified proteins. A reaction without protein was used as a negative control. A solution of *n*-butanol–pyridine acetate (1:2) was added to the reaction mixture in a 1:1 percentage to extract the lipid products, and after centrifugation at 17,000 $\times$ *g* for 3 min, the products were analyzed by thin-layer chromatography (TLC) using *n*-butanol, acetic acid, water, and pyridine (15:3:12:1) as the mobile phase for 2 h. The lipid spots were visualized using iodine vapor.

Peptidoglycan purification. Cell wall isolation was performed as described previously (18). Briefly, cells were grown in the presence of the respective antibiotics and inducer concentration up to an OD_{620} of 0.3, harvested by centrifugation, rapidly chilled in an ice-ethanol bath, and boiled in 4% SDS for 30 min. The cells were disrupted using 106-mm glass beads (sigma) and subsequently treated with DNase (10 μg/ml; Sigma-Aldrich), RNase (50 μg/ml; Sigma-Aldrich), and trypsin (200 μg/ml; Worthington Biochemical Corporation, USA). Teichoic acids were removed by treatment with 49% hydrofluoric acid (Merck, Germany) for 48 h at 4°C. The peptidoglycan was lyophilized.

Muropeptide analysis by RP-HPLC. Identical amounts of peptidoglycan of each sample were digested with mutanolysin (1 mg/ml; Sigma). This process was repeated in triplicate for each condition. The resulting muropeptides were reduced with sodium borohydride powder (Sigma) and separated by reverse-phase high-performance liquid chromatography (RP-HPLC) using a Hypersil octyldecyl silane (Runcorn, Cheshire, UK) column and a linear gradient from 5% to 30% methanol in 100 mM sodium phosphate buffer, pH 2.5, at a flow rate of 0.5 ml/min as described previously (18), using a Shimadzu Prominence system and Shimadzu LC solution software. The peaks of the chromatograms were identified by assessing the relative retention times according to previous work (18, 19). The peaks were integrated, and the values are presented as the area percentages of the total area of the chromatogram (18, 28). The baseline used for the integration of the individual peaks was the same as the one used for the whole chromatogram. The values presented are the means from three independent replicates, and the standard deviation values were calculated.

SUPPLEMENTAL MATERIAL

Supplemental material for this article may be found at https://doi.org/10.1128/AAC.00957-19.

SUPPLEMENTAL FILE 1, PDF file, 1.5 MB.

ACKNOWLEDGMENTS

This work was supported by the Fundação para a Ciência e a Tecnologia (FCT) through grants PTDC/BIA-MIC/3195/2012 (awarded to H.L.) and grants PTDC/FIS-NAN/

0117/2014 and PTDC/BIA-MIC/31645/2017 (awarded to R.G.S.); by project UID/Multi/04378/2019 (Unidade de Ciências Biomoleculares Aplicadas-UCIBIO), funded by FCT/MCTES; by project LISBOA-01-0145-FEDER-007660 (Microbiologia Molecular, Estrutural e Celular), funded by FEDER through COMPETE2020—Programa Operacional Competitividade e Internacionalização (POCI); by national funds through FCT; by project ONEIDA (LISBOA-01-0145-FEDER-016417), cofunded by FEEI (Fundos Europeus Estruturais e de Investimento) from the Programa Operacional Regional Lisboa 2020; and by national funds from FCT. Funding was also provided by European Society of Clinical Microbiology and Infectious Diseases research grant 2015, awarded to R.G.S. B.V.G., T.A.F., and I.R.G. were supported by fellowships SFRH/BD/131623/2017, SFRH/BD/36843/2007, and SFRH/BD/70162/2010, respectively. J.S.D. acknowledges the National NMR Network (PTNMR) and Infrastructure Project ROTEIRO/0031/2013-PINFRA/22161/2016 (cofinanced by FEDER through COMPETE 2020, POCI, PORL, and FCT through PIDDAC).

We thank L. J. Mota and coworkers for providing the BACTH system and for technical and scientific advice, S. Filipe for use of the HPLC equipment, and A. Tomasz and L. J. Mota for critical reading of the manuscript.

B.V.G., R.P., R.L., T.A.F., and I.R.G. performed the experiments. J.S.D. performed the structure analysis. A.M.L., H.D.L., J.S.D. and R.G.S. conceived of the study. B.V.G., R.P., R.L., T.A.F., A.M.L., J.S.D., and R.G.S. designed the research. B.V.G., A.M.L., H.D.L., J.S.D., and R.G.S. wrote the paper with the contribution of R.P.

We declare no competing financial interests.

REFERENCES

1. Bouhss A, Trunkfield AE, Bugg TD, Mengin-Lecreulx D. 2008. The biosynthesis of peptidoglycan lipid-linked intermediates. FEMS Microbiol Rev 32:208–233. https://doi.org/10.1111/j.1574-6976.2007.00089.x.
2. Vollmer W. 2008. Structural variation in the glycan strands of bacterial peptidoglycan. FEMS Microbiol Rev 32:287–306. https://doi.org/10.1111/j.1574-6976.2007.00088.x.
3. Bera A, Herbert S, Jakob A, Vollmer W, Gotz F. 2005. Why are pathogenic staphylococci so lysozyme resistant? The peptidoglycan O-acetyltransferase OatA is the major determinant for lysozyme resistance of *Staphylococcus aureus*. Mol Microbiol 55:778–787. https://doi.org/10.1111/j.1365-2958.2004.04446.x.
4. Herbert S, Bera A, Nerz C, Kraus D, Peschel A, Goerke C, Meehl M, Cheung A, Gotz F. 2007. Molecular basis of resistance to muramidase and cationic antimicrobial peptide activity of lysozyme in staphylococci. PLoS Pathog 3:e102. https://doi.org/10.1371/journal.ppat.0030102.
5. Figueiredo TA, Sobral RG, Ludovice AM, Almeida JM, Bui NK, Vollmer W, de Lencastre H, Tomasz A. 2012. Identification of genetic determinants and enzymes involved with the amidation of glutamic acid residues in the peptidoglycan of *Staphylococcus aureus*. PLoS Pathog 8:e1002508. https://doi.org/10.1371/journal.ppat.1002508.
6. Ngadjeua F, Braud E, Saidjalolov S, Iannazzo L, Schnappinger D, Ehrt S, Hugonnet JE, Mengin-Lecreulx D, Patin D, Etheve-Quelquejeu M, Fonvielle M, Arthur M. 2018. Critical impact of peptidoglycan precursor amidation on the activity of L,D-transpeptidases from Enterococcus faecium and Mycobacterium tuberculosis. Chemistry 24:5743–5747. https://doi.org/10.1002/chem.201706082.
7. Figueiredo TA, Ludovice AM, Sobral RG. 2014. Contribution of peptidoglycan amidation to beta-lactam and lysozyme resistance in different genetic lineages of *Staphylococcus aureus*. Microb Drug Resist 20:238–249. https://doi.org/10.1089/mdr.2014.0042.
8. Munch D, Roemer T, Lee SH, Engeser M, Sahl HG, Schneider T. 2012. Identification and in vitro analysis of the GatD/MurT enzyme-complex catalyzing lipid II amidation in *Staphylococcus aureus*. PLoS Pathog 8:e1002509. https://doi.org/10.1371/journal.ppat.1002509.
9. Massiere F, Badet-Denisot MA. 1998. The mechanism of glutamine-dependent amidotransferases. Cell Mol Life Sci 54:205–222. https://doi.org/10.1007/s000180050145.
10. Mouilleron S, Golinelli-Pimpaneau B. 2007. Conformational changes in ammonia-channeling glutamine amidotransferases. Curr Opin Struct Biol 17:653–664. https://doi.org/10.1016/j.sbi.2007.09.003.
11. Raushel FM, Thoden JB, Holden HM. 1999. The amidotransferase family of enzymes: molecular machines for the production and delivery of ammonia. Biochemistry 38:7891–7899. https://doi.org/10.1021/bi990871p.
12. Smith CA. 2006. Structure, function and dynamics in the Mur family of bacterial cell wall ligases. J Mol Biol 362:640–655. https://doi.org/10.1016/j.jmb.2006.07.066.
13. van Heijenoort J. 2001. Recent advances in the formation of the bacterial peptidoglycan monomer unit. Nat Prod Rep 18:503–519. https://doi.org/10.1039/a804532a.
14. Karimova G, Pidoux J, Ullmann A, Ladant D. 1998. A bacterial two-hybrid system based on a reconstituted signal transduction pathway. Proc Natl Acad Sci U S A 95:5752–5756. https://doi.org/10.1073/pnas.95.10.5752.
15. Moreira IS, Fernandes PA, Ramos MJ. 2007. Hot spots—a review of the protein-protein interface determinant amino-acid residues. Proteins 68:803–812. https://doi.org/10.1002/prot.21396.
16. Gardete S, Kim C, Hartmann BM, Mwangi M, Roux CM, Dunman PM, Chambers HF, Tomasz A. 2012. Genetic pathway in acquisition and loss of vancomycin resistance in a methicillin resistant *Staphylococcus aureus* (MRSA) strain of clonal type USA300. PLoS Pathog 8:e1002505. https://doi.org/10.1371/journal.ppat.1002505.
17. Qiao Y, Srisuknimit V, Rubino F, Schaefer K, Ruiz N, Walker S, Kahne D. 2017. Lipid II overproduction allows direct assay of transpeptidase inhibition by beta-lactams. Nat Chem Biol 13:793–798. https://doi.org/10.1038/nchembio.2388.
18. de Jonge BL, Chang YS, Gage D, Tomasz A. 1992. Peptidoglycan composition in heterogeneous Tn551 mutants of a methicillin-resistant Staphylococcus aureus strain. J Biol Chem 267:11255–11259.
19. Ornelas-Soares A, de Lencastre H, de Jonge B, Gage D, Chang YS, Tomasz A. 1993. The peptidoglycan composition of a *Staphylococcus aureus* mutant selected for reduced methicillin resistance. J Biol Chem 268:26268–26272.
20. Morlot C, Straume D, Peters K, Hegnar OA, Simon N, Villard A-M, Contreras-Martel C, Leisico F, Breukink E, Gravier-Pelletier C, Le Corre L, Vollmer W, Pietrancosta N, Håvarstein LS, Zapun A. 2018. Structure of the essential peptidoglycan amidotransferase MurT/GatD complex from Streptococcus pneumoniae. Nat Commun 9:3180. https://doi.org/10.1038/s41467-018-05602-w.
21. Noldeke ER, Muckenfuss LM, Niemann V, Muller A, Stork E, Zocher G, Schneider T, Stehle T. 2018. Structural basis of cell wall peptidoglycan amidation by the GatD/MurT complex of Staphylococcus aureus. Sci Rep 8:12953. https://doi.org/10.1038/s41598-018-31098-x.

22. Boniface A, Bouhss A, Mengin-Lecreulx D, Blanot D. 2006. The MurE synthetase from Thermotoga maritima is endowed with an unusual D-lysine adding activity. J Biol Chem 281:15680–15686. https://doi.org/10.1074/jbc.M506311200.
23. Gordon E, Flouret B, Chantalat L, van Heijenoort J, Mengin-Lecreulx D, Dideberg O. 2001. Crystal structure of UDP-N-acetylmuramoyl-L-alanyl-D-glutamate: meso-diaminopimelate ligase from Escherichia coli. J Biol Chem 276:10999–11006. https://doi.org/10.1074/jbc.M009835200.
24. Ruane KM, Lloyd AJ, Fulop V, Dowson CG, Barreteau H, Boniface A, Dementin S, Blanot D, Mengin-Lecreulx D, Gobec S, Dessen A, Roper DI. 2013. Specificity determinants for lysine incorporation in Staphylococcus aureus peptidoglycan as revealed by the structure of a MurE enzyme ternary complex. J Biol Chem 288:33439–33448. https://doi.org/10.1074/jbc.M113.508135.
25. Leisico F, Vieira DV, Figueiredo TA, Silva M, Cabrita EJ, Sobral RG, Ludovice AM, Trincao J, Romao MJ, de Lencastre H, Santos-Silva T. 2018. First insights of peptidoglycan amidation in Gram-positive bacteria—the high-resolution crystal structure of *Staphylococcus aureus* glutamine amidotransferase GatD. Sci Rep 8:5313. https://doi.org/10.1038/s41598-018-22986-3.
26. Larkin MA, Blackshields G, Brown NP, Chenna R, McGettigan PA, McWilliam H, Valentin F, Wallace IM, Wilm A, Lopez R, Thompson JD, Gibson TJ, Higgins DG. 2007. Clustal W and Clustal X version 2.0. Bioinformatics 23:2947–2948. https://doi.org/10.1093/bioinformatics/btm404.
27. Oshida T, Tomasz A. 1992. Isolation and characterization of a Tn*551*-autolysis mutant of *Staphylococcus aureus*. J Bacteriol 174:4952–4959. https://doi.org/10.1128/jb.174.15.4952-4959.1992.
28. Sobral RG, Ludovice AM, Gardete S, Tabei K, De Lencastre H, Tomasz A. 2003. Normally functioning murF is essential for the optimal expression of methicillin resistance in Staphylococcus aureus. Microb Drug Resist 9:231–241. https://doi.org/10.1089/107662903322286436.
29. Kraemer GR, Iandolo JJ. 1990. High-frequency transformation of Staphylococcus aureus by electroporation. Curr Microbiol 21:373. https://doi.org/10.1007/BF02199440.